Numerical Simulations of Population Transfer in Helium with Intense Ultrashort Chirped Laser Pulses

by

Donald Rex Planalp Jr

University of Colorado Boulder: Department of Physics

Defense Date: March 30, 2022

Committee Members

Thesis Advisor: Prof. Andreas Becker, Dept. of Physics

Honors Council Member: Prof. Paul Beale, Dept. of Physics

Outside Reader: Prof. Harrison Stalvey, Dept. of Mathematics

Abstract

The interaction of light with quantum systems is an important probe used to control matter and chemical reactions. One manner in which light is used to control matter is to change the population of a quantum state from a given initial state to a desired final state. In this thesis we consider how intense ultrashort linearly chirped laser pulses can be used to control population transfer in Helium. The study is conducted by numerically solving the time dependent Schrödinger equation. To understand trends in the Helium state population after interacting with the laser pulse, we consider how the frequency of the pulse varies in time. Comparing the time dependent frequency curve to various resonant population transfer frequencies, we see that this model can both explain and predict several characteristics of the final population, where we use the $3p$ population as a case study.

Acknowledgements

Throughout writing this thesis and during my undergraduate research with the Ultrafast AMO Theory group of Dr. Andreas Becker, I have received a great deal of support and assistance.

I would first like to give a special thanks to my thesis advisor Dr. Andreas Becker for giving me the opportunity to work with his group. Joining his research group during the Fall of 2020 meant that there were many complications due to the COVID-19 pandemic. Without Professor Becker's flexibility and support during this chaotic period, this thesis would not be possible. I would also like to thank Professor Becker and the graduate students in his group, especially Yonas Gebre, for their assistance during the project itself. Without their assistance I would not have been able to navigate neither the research nor the writing of this thesis.

Finally I would like to thank all of my friends and family back home. Without the encouragement of my mother and father, I would not have had the confidence and determination necessary to undertake this research project.

Contents

Figures

Figure

Chapter 1

Introduction

1.1 Background

The control of population transfer in quantum systems is an important topic of study and has applications in the field of Atomic, Molecular, and Optical physics and beyond. Examples include the ability to prepare specific states for quantum information experiments in which decoherence issues can occur [1], as well as the potential to control chemical reaction rates via chirped lasers [2]. While there are many well-studied population transfer techniques [3, 4], rapid adiabatic passage (RAP) is efficient and can be achieved via a time-dependent resonant frequency, or a chirped laser pulse [5]. Very recently it has been shown by Saalman et al.[6] that the ionization of Helium atoms upon interaction with an intense laser can be modulated using a linearly chirped pulse. Specifically, they showed that ionization is suppressed for the negative chirp and promoted for positive . The result is that although Helium would otherwise ionize in the presence of a laser, this ionization can be either enhanced or suppressed.

There has been recent progress in producing intense, ultrashort, high-frequency pulses at a wide range of wavelengths. Research into the generation of these ultrashort pulses has been conducted using free-electron lasers as well as utilizing table-top systems [7, 8]. As a result of this technological progress, there is a newfound interest into what theoretical predictions we can make, and how they are relevant to new opportunities in labs. As the experimental possibilities broaden, it becomes important to conduct theoretical analysis on where the labs may be investigating in the near future. Further insight into the precise ionization or more general quantum state control

via an ultrashort linearly chirped pulse is an important topic of study, due to the wide range of applications in both atomic and molecular manipulation. This allows experimental researchers to fully take advantage of our predictions, and to confirm or falsify our results.

Motivated by the results of Saalmann et al. [6], in this thesis we investigate population transfer in Helium using intense ultrashort laser pulses with a linear chirp. This investigation is done via numerically solving the time dependent Schrödinger equation (TDSE) in the semi-classical limit. The purpose of this study is to take a closer look at how intense, linearly chirped pulses can be used to control the excitation/ionization of Helium atoms and to probe for what new mechanisms arises when very short pulses are used. Shorter pulses, as we will see, present new possibilities for physics due to the broad width of the energy spectrum of the pulse, allowing a wider variety of population transfer between the states. Furthermore, we intend to investigate new patterns arising due to ultrashort pulses, and analyze the mechanisms for ionization enhancement and suppression caused by pulses with either negative or positive chirp.

1.2 Methods

1.2.1 Quantum State Population

The purpose of this study is to investigate the ionization and population transfer of Helium when interacting with a laser pulse. To this end we first review the basic topics of quantum states, and the transfer of population. Both of these topics will be integral to the results discussed later on.

According to quantum mechanics a system can be in multiple distinct states simultaneously. The system is then said to be in a superposition of those states. Mathematically this amounts to expressing the state as a sum over a discrete basis, ϕ_n, and/or an integral over a continuous one, $\phi(\mathbf{k})$, which can be written as:

$$\psi(x) = \sum_n c_n \phi_n(x) \tag{1.1}$$

or

$$\psi(\mathbf{r}) = \frac{1}{(2\pi)^{\frac{3}{2}}} \int_{-\infty}^{\infty} \phi(\mathbf{k}) e^{-i\mathbf{k}\cdot\mathbf{r}} d\mathbf{k} \tag{1.2}$$

It should be noted that instead of working with abstract kets $|\psi\rangle$, we work with the position space representation $\psi(\mathbf{r}) = \langle \mathbf{r}|\psi\rangle$, also called the position space wavefunction. A common basis used to expand the wave function of a system is the set of eigenfunctions of the total energy operator, which are found by solving the time independent Schrödinger equation (TISE). This is a desirable choice because the total energy of a state is a useful quantity, and the time evolution becomes simple since energy eigenstates evolve via by a simple phase factor $e^{-\frac{iEt}{\hbar}}$ where E is the energy of the discrete or continuous state. In the examples above we have a discrete superposition of 1D energy eigenstates, and a continuous superposition of 3D free particle energy eigenstates. To accommodate the discrete case to higher dimensions, we would need to sum over all allowed combinations of three different quantum numbers. For atoms, the quantum state is identified by the three quantum numbers n, l, m. The expansion coefficients now depend on all three quantum numbers, so $c_n \rightarrow c_{nlm}$. In general, the expansion coefficients can be complex valued, and their magnitude squared yields the probability of the superposition state to have energy E_{nlm} upon measurement. This is the mathematical value that we use to denote the population of a state. The population of a state (nlm) is, hence, the probability of collapsing into the (nlm) state after energy is measured. Throughout this thesis we use the electron configuration notation where the state (nlm) is written as nx_m where for $l = 0, 1, 2, 3 \ldots = s, p, d, f \ldots$ So the ground state (100) is now written as $1s$, where $m = 0$ is implied.

Next we consider the transfer of population. In the examples above the wave functions are written at a single instant in time, lacking any time evolution. However, the expansion coefficients c_{nlm} could change over time. Without any external perturbation the coefficients evolve as mentioned above, only changing by a phase factor. However when we have an external perturbation, the magnitude of the coefficients may vary. For example, lets suppose the wavefunction starts in the ground state $1s$, so $c_{100} = 1$ and all other expansion coefficients are zero. After the system interacts

with the external perturbation the expansion coefficients may change to $c_{100} = 0.5$ and $c_{200} = 0.5$. In that case the population of (or probability to find the system in) the $1s$ state has decreased, while the population of the $2s$ state has increased. We would then say that population was transferred from the ground state into the first excited state.

Population transfer between two specific states can be stimulated via interaction with a classical electromagnetic wave resonant with the coupling frequency between said states. The coupling frequency is defined as $\omega_c = \frac{|\Delta E|}{\hbar}$, where ΔE is the difference in energy between the two states. In this way, by subjecting the system to a monochromatic light source one can transfer population from one state to another efficiently. This basic principle of population transfer due to the frequency of the laser pulse resonating with the coupling frequency is necessary for describing some of the population results we report for very short pulses. Later when defining the form of the laser pulse, we will assume the electromagnetic wave to be linearly polarized. This implies that $|\Delta m| = 0$, which can be understood by considering that a linearly polarized pulse does not have a net angular momentum. Since there is no z-component of angular momentum in the light which might change the angular momentum of the atom, the quantum number associated with the z-component of angular momentum (m) will not change upon interaction with such a pulse. Since we are considering the Helium atom in the $1s$ state where $m = 0$ as the initial state in our studies, all of the population transferred to excited states appears in states with $m = 0$.

1.2.2 Semiclassical approximation

To approach the problem of describing the interaction of Helium with an external electromagnetic field, we must first make some basic assumptions about the system which will shape how we approach a solution. These approximations are the semiclassical approximation for light, the non-relativistic Schrödinger equation, and finally the single-active electron approximation (SAE) which together simplify the problem and make it practical for numerical simulations.

The first approximation is the semiclassical approximation for light. In the modern treatment of light-matter interactions one would normally need to apply principles of quantum field theory in

order to take into account the quantization of the electromagnetic field. This would not be incorrect, however there is a simplifying assumption one can make. Since we are working with intense laser pulses with an intensity of the order of $10^{15}\frac{W}{cm^2}$ or greater, the number of photons in the laser field is incredibly large. In this large photon limit, the discrete nature of the electromagnetic field becomes obscured and can be replaced by a continuous description. This description allows us to model the electromagnetic field field as an oscillating electromagnetic wave which solves Maxwell's equations. Thus instead of taking into account a myriad of photons interacting with the system, we simply treat the electromagnetic field as a single cohesive object. As we will see, the actual mathematical objects we use to describe light-matter interactions are the associated potential of the oscillating EM wave, not the electric or magnetic fields themselves.

1.2.3 Schrödinger Equation

The second approximation is the use of the Schrödinger equation. The Schrödinger equation relates to a non-relativistic description and it does not take spin into consideration. If we were to attempt a relativistic description we would need to seek solutions to the Dirac equation. However, for the laser-matter interaction we are simulating, we do not expect electron momentum expectation values to approach a value which would produce inconsistencies with special relativity. Since we are interested in the resultant population distributions of the system, it is also not necessary to take spin into account, otherwise we might seek solutions to the Pauli equation. Thus, in the non-relativistic limit without spin, we can apply the time dependent Schrödinger equation,

$$i\partial_t\psi(\mathbf{r},t) = H\psi(\mathbf{r},t), \tag{1.3}$$

where H denotes the Hamiltonian of the system. Also, in the above equation and hereafter we choose atomic units where $m_e = \hbar = e = 1$ which allows us to work in dimensionless units when solving the Schrödinger equation numerically.

1.2.4 Single-Active Electron Model

The final approximation is the single-active electron approximation (SAE). Since the Helium atom we are considering is not initially ionized, we would need to take into account the dynamics of both electrons, and possibly deal with multi-electron effects. However, modeling the dynamics of both electrons increases the computational resources necessary to conduct an accurate simulation. We therefore take advantage of the SAE approximation, in which only one electron interacts with the laser pulse, treating the other electron as being fixed in its initial state. This reduces the problem to modeling one electron dynamics, allowing a similar numerical approach to solving the TDSE in a similar fashion to that of Hydrogen. Since we are assuming that only one electron is interacting with the laser, we need to modify the Coulomb potential in order for the numerical results from the single particle physics model to approximately simulate the correct physics for the physical two electron system. The general form of this potential is taken from [6], and is given by:

$$V_{SAE}(r) = -\frac{C_0}{r} - Z_c\frac{e^{-cr}}{r} - a_1 e^{-b_1 r}, \tag{1.4}$$

where r refers to the radial distance from the origin. The first term in the potential is the normal long-range Coulomb potential, while the second and third terms model the short-range effects due to the presence of the second electron. The parameter C_0 is there to take into account for a non-zero net charge. The second term is in the form of a Yukawa potential, and can be interpreted as a screening effect caused by the static second electron which can be modeled via a reduced effective charge of the nucleus. The final term takes into account the specifics of the interaction between the static electron and the dynamic electron. The various parameters appearing in the above equation must be fit in order to approximate the full physics. The parameters used for the simulations were determined in [9] using density functional theory (DFT). The resulting potential is shown below

$$V(r) = -\frac{1}{r} - \frac{e^{-2.0329}}{r} - 0.3953e^{-6.1805r}. \tag{1.5}$$

The validity of this potential has been shown through a study on the ionization of Helium in [10]. We have therefore assembled all of the assumptions made to conduct this study, now we need

to discuss the details of the equation which we will need to solve numerically.

1.2.5 Light-Matter Interaction

In order to model the interaction of the single-active electron with light, we must include light-matter interaction in the Schrödinger equation as an additional term in the Hamiltonian. As noted previously, we do not work with the electric or magnetic fields directly, but the scalar and vector potentials. Due to the gauge symmetry present in the semiclassical description of light, we have some freedom for how we wish to define the potentials. However this choice has no impact on the physics as long as the proper gauge conditions are met. Two common choices are the length and velocity gauges, which are named after the observables appearing in the corresponding interaction terms in the Hamiltonian. In the length gauge the electromagnetic potential energy term is $U = -\mathbf{r}\cdot\mathbf{E}(\mathbf{r},t)$. In the velocity gauge the term becomes $U = -\mathbf{p}\cdot\mathbf{A}(\mathbf{r},t)$. For the purposes of this study we chose the velocity gauge, since there is evidence that for high intensity laser simulations, calculations performed in velocity gauge are more efficent than those with length gauge [11]. With this modification to the Hamiltonian, the Schrödinger equation takes the following form:

$$i\partial_t\psi(\mathbf{r},t) = (H_0 - \mathbf{p}\cdot\mathbf{A}(\mathbf{t}))\psi(\mathbf{r},t), \tag{1.6}$$

where H_0 now denotes the field-free Hamiltonian, containing both the electrostatic SAE potential as well as the kinetic energy of the electron. All that remains is to discuss the numerical approach taken to solving this form of the Schrödinger equation.

1.2.6 Numerical Scheme

The numerical scheme used to solve the problem is a 4th order finite difference method to solve for the energy eigenstates of Helium, as well as the Crank-Nicholson scheme to propagate the wave function in time. The finite difference method works by projecting the operators, such as the Hamiltonian and potential energy, onto a discrete grid in space. This discretization is done in spherical coordinates, since a spherical coordinate system is best suited for describing atomic

wave functions. To be concrete, we used a 950 a.u sized grid with a 0.05 a.u step size in space. In order to show how this discretization works we take the example of a 1D system using Cartesian coordinates, which illustrates the basic ideas. We start with the 1D time independent Schrödinger equation in atomic units

$$-\frac{1}{2}\frac{d^2\psi}{dx^2} + V(x)\psi(x) = E\psi(x). \tag{1.7}$$

To construct a discrete difference equation from this continuous differential equation we apply the central finite difference discretization of the differential operator. Conceptually we take the continuous position variable x and replace it by a set of discrete grid points x_n where the index n refers to a particular position $x_n = n\Delta x$. If we make the grid spacing Δx sufficiently small we can approximate:

$$\frac{d^2\psi}{dx^2} \approx \frac{\psi_{n+1} - 2\psi_n + \psi_{n-1}}{\Delta x^2}, \tag{1.8}$$

where $\psi_n = \psi(x_n)$. This also implies that the potential $V(x)$ becomes discrete as well, where $V_n = V(x_n)$. Since the differential operator is now a linear combination of discrete ψ_n values, we can rewrite the Hamiltonian acting on the wave function as a matrix equation; namely, the Hamiltonian matrix multiplying the vector containing all ψ_n values. Using this matrix equation we can solve for the eigenvalues and discretized eigenfunctions of the Hamiltonian matrix, which for our purposes is done most efficiently with the PETSc for python package [12].

In order to solve for the time propagation of the wave function, we utilize a 4th order Crank-Nicholson scheme. The temporal resolution for propagation is 0.05 a.u. in order to ensure accuracy. To avoid interference due to the wave function reflecting off the boundary of the grid, we apply an absorbing boundary condition at the end of the grid. The Crank-Nicholson scheme has the advantage of effectively being an average between the forward and backward Euler propagation methods. This not only provides stability and accuracy, but ensures that the wave function stays properly normalized as it is updated for each time interval.

To set the propagation scheme, we make use of the time evolution operator. The time evolution operator can be derived directly from the Schrödinger equation, and takes the form

$U(t,t') = e^{-iH(t)(t-t')}$. The action of the time evolution operator on a wave function is given by:

$$U(t,t')\psi(\mathbf{r},t) = \psi(\mathbf{r},t'). \tag{1.9}$$

Thus, as the name implies, given two times t and t' one can evolve a wave function from t to t' by acting with the operator on the state. It should be noted that in order to flip the direction of time propagation we would need to introduce a minus sign in the exponential, effectively allowing us to move a wave function backards in time. Since we are interested in propagating the wave function sequentially over very small time steps, we want to take the limit $\lim_{t'\to t}$. This recovers the differential time evolution operator, $U(t,t+dt) = e^{-iH(t)dt)}$, where $t' = t+dt$. For the purpose of numerical simulation dt is not a differential quantity, but one that we take sufficiently small enough. As stated earlier the temporal resolution is 0.05 a.u, which implies $dt = 0.05$ for the calculation. From here all we need to do in order to arrive at the Crank-Nicholson scheme is to apply the differential time evolution operator to the wave function using a forward and a backward step. Specifically, we take the wave function $\psi(\mathbf{r},t)$ and apply the differential time evolution operator over a half step $\frac{dt}{2}$. According to the above equation, this should yield $\psi(\mathbf{r},t+\frac{dt}{2})$. Now we take the wave function at the next full time step $\psi(\mathbf{r},t+dt)$ and apply a half step backwards, flipping the sign in the exponential. This should also yield $\psi(\mathbf{r},t+\frac{dt}{2})$ as well. Thus we end up with the equation:

$$e^{\frac{iH(t)dt}{2}}\psi(\mathbf{r},t_{n+1}) = e^{\frac{-iH(t)dt}{2}}\psi(\mathbf{r},t_n). \tag{1.10}$$

This equation defines the Crank-Nicholson scheme by relating the wave function at a time t to a later time $t+dt$. However, we can use the fact that dt is small to simplify the equation. Since we allow dt to be sufficiently small, we can Taylor expand each exponential to first order in dt, resulting in the system of linear equations:

$$[\hat{I} + \frac{idt}{2}H(t_{n+1/2})]\psi(\mathbf{r},t_{n+1}) = [\hat{I} - \frac{idt}{2}H(t_{n+1/2})]\psi(\mathbf{r},t_n), \tag{1.11}$$

where now t_{n+1} refers to the wave function at the next full time step dt. We are now presented with a system of linear equations which can be solved numerically for the updated wave function.

The code used to solve this linear system, as well as the one constructed to solve for the energy eigenstates, was provided by graduate students in the Becker group. This code is written in Python, and to speed up solving the linear system of equations, PETSc for Python is used which paralellizes the code to take advantage of multi-CPU computers in the JILA photon cluster. The code is further optimized where appropriate to use Cython which allows pure python code to be compiled as C, increasing speed and efficiency [13].

1.2.7 Chirped Pulses

In accordance with the definitions used by Saalman et al. in their study [6], we adopt the same mathematical form of the chirped pulse. The vector potential is set using a sinusoidal carrier wave modulated by a Gaussian envelope. This envelope ensures that the pulse is localized in time, the duration of the pulse is controlled and the total energy remains the same. The exact mathematical form of the vector potential is given by:

$$\mathbf{A}(t,\beta) = A_\beta e^{-2ln\frac{2t^2}{T_\beta^2}} cos(\phi(t) - \delta)\hat{z}. \tag{1.12}$$

Before proceeding we must define some of the parameters present in this equation. First, we have defined the peak amplitude of the pulse A_β which is related to the unchirped peak amplitude $A_0 \propto I$. We have also defined the carrier-envelope phase δ, which is the difference in phase between the center of the cosine function and the Gaussian envelope. Most importantly, the magnitude of the chirp parameter β controls the strength of the chirp, while the sign changes the chirp direction. The chirp parameter also has an effect on the period and amplitude of the pulse. The mathematical form of these relationships is given as follows:

$$T_\beta = T\sqrt{1+\beta^2} \tag{1.13}$$

and

$$A_\beta = A_0(1+\beta^2)^{-1/4}. \tag{1.14}$$

We have also defined the unchirped period T to be $T = \frac{2\pi N}{\omega_0}$, where N is the number of cycles in the unchirped pulse. In the above equations we see some of the key changes that occur due to the

introduction of the chirp parameter. Namely, β causes the Gaussian envelope to be widened in time, and a reduction in the peak amplitude. The net result is that the Gaussian envelope is effectively stretched out so that the pulse energy remains the same. Another important quantity in the vector potential is ϕ, whose derivative with respect to time is defined as the instantaneous frequency of the pulse. Since the pulse is linearly chirped, the instantaneous frequency varies linearly in time. The frequency as a function of chirp parameter and time is given by:

$$\omega_\beta(t) = \omega_0 + \frac{4t\beta ln2}{(\beta^2+\beta)T^2}. \tag{1.15}$$

The linear dependence of ω on time is explicit here, with a y-intercept of ω_0. For the calculations we assumed the Helium atom is initially in its ground state, and the unchirped frequency ω_0 is set to the $1s-2p$ coupling frequency. This coupling is defined as $E_{2p}-E_{1s}$ in atomic units, which is about 0.815 a.u. in the single active-electron-model used. While the chirp parameter is free to take on both positive and negative values, we restrict our study to $\beta \in [-4,4]$, which is the range that Saalman et al. used as well.

In order to visualize the impact that the chirp parameter has on the pulse itself, in Fig. 1.1 we have plotted examples of pulses with zero, positive, and negative chirp parameter. Three different pulses are plotted for 2 cycles in unchirped pulses. We are able to observe some of the key differences between a positive and negative chirp. The pulse with positive β causes the instantaneous frequency to increase over time, while the one with negative β causes it to decrease over time. As stated previously, the coupling frequency is obtained at the center of the pulse, i.e. $t = 0$. It should also be noted that the stretching of the pulse is dependent on the magnitude of β, independent of the direction/sign. It can also be seen that the stretching also reduces the peak amplitude of the pulse, with $|\beta| = 1$ resulting in a reduction in peak amplitude by 25 percent.

1.2.8 Laser Pulse Spectrum

In order to understand how shortening the duration of the pulse creates opportunities for new physics, we need to discuss the Fourier transform. The Fourier transform takes an input function

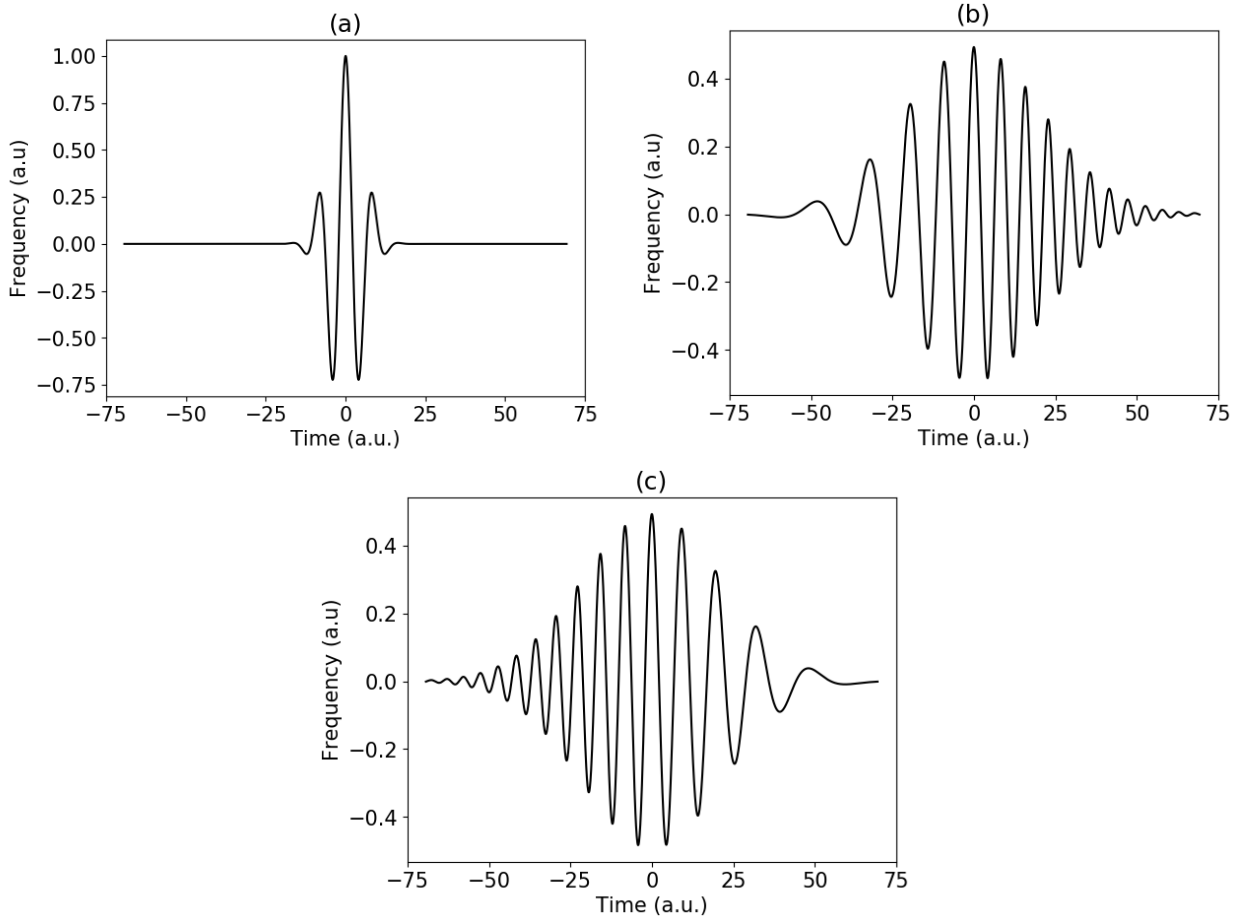

Figure 1.1: Laser pulses with (a) zero, (b) positive, and (c) negative chirp. The chirp parameter β was chosen to be $\beta = \pm 1$ in panels (b) and (c), respectively.

$f(t)$, and produces its Fourier transform function $\mathcal{F}[f(t)] = F(\omega)$. The mathematical relationships between $f(t)$ and $F(\omega)$ is given by

$$F(\omega) = \frac{1}{\sqrt{2\pi}} \int_{-\infty}^{\infty} f(t) e^{-i\omega t} dt \tag{1.16}$$

and

$$f(t) = \frac{1}{\sqrt{2\pi}} \int_{-\infty}^{\infty} F(\omega) e^{i\omega t} d\omega, \tag{1.17}$$

where the second equation is defined as the inverse Fourier transform $\mathcal{F}^{-1}[F(\omega)]$. We also see that the imaginary unit i appears in the term $e^{-i\omega t}$ which implies that if $f(t)$ is real, $F(\omega)$ will (in general) be complex. Similar to the previous discussion on electron states, we can interpret the inverse Fourier transform as a continuous basis state decomposition of $f(t)$ with $F(\omega)$ acting as the expansion coefficients. Since these basis states are also states of definite frequency/energy ω, $F(\omega)$ contains information about the distribution of frequencies/energies within the pulse. Although the population transfer between states is most likely promoted when the frequency is near the coupling between those states, it is important to understand the frequency distribution of the pulse.

For our purposes, the function that modulates the duration of the pulse in time is the envelope function $f_\beta(t) = e^{-2ln\frac{2t^2}{T_\beta^2}}$. In order to extract information about how the frequency distribution changes as we increase or decrease the pulse duration, we need to characterize the temporal and spectral widths of the pulse. In the temporal domain the envelope is a Gaussian with a width that can be defined via its Full Width at Half Maximum (FWHM). A graphical representation of FWHM is shown in Figure 1.2.

Since the Fourier transform of a Gaussian is also a Gaussian, via the FWHM we have also established the necessary definitions to characterize the width of $F(\omega)$ which we refer to as spectral width. The FWHM for the temporal envelope is proportional to T_β, while the FWHM for the Fourier transform is inversely proportional to T_β. Since $T_\beta \propto N$, we can directly relate the behavior of the FWHM's to the number of pulse cycles, which is shown in Figure 1.3

We see that for small N, the spectral width is very large while the temporal width is small. A wide spectral width allows for population transfer between states to happen over a longer time

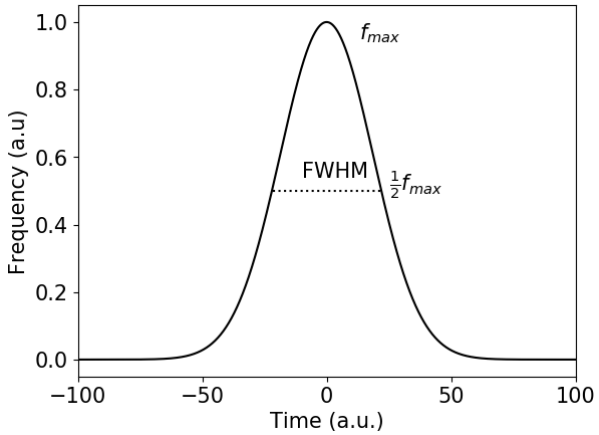

Figure 1.2: A Gaussian function labeled to display the definition of the FWHM.

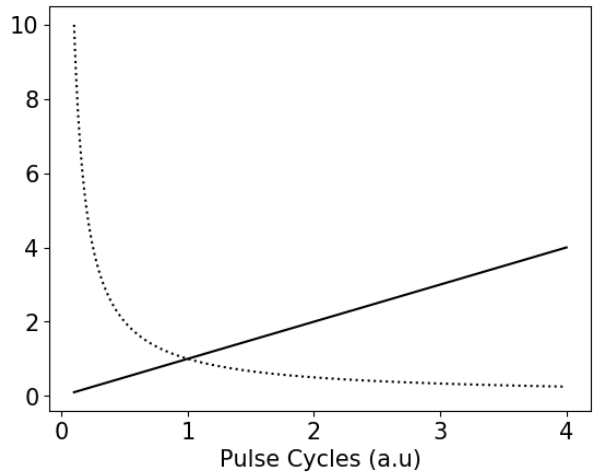

Figure 1.3: The FWHM of the temporal and spectral envelopes plotted against number of pulse cycles N

during the pulse. This is because the frequency distribution is more likely to overlap with a coupling frequency between any two particular states. For large N we see that the spectral width goes to zero. This is consistent with the infinitely long pulse limit, at which the pulse has a perfectly well defined frequency, and the spectral Gaussian becomes a delta function. While we are interested mainly in what happens as the pulse duration decreases, we must ensure that our results are consistent with the results obtained in [6] for the long pulse case.

In [6], Saalman et al. concludes that the ionization of Helium can be controlled depending on the sign of the chirp parameter used in the pulse. In Figure 1.4 we compare their result (left) with the results of our simulation (right, for similar pulse parameters). We see that the ionization is promoted for $\beta > 0$ and suppressed for $\beta < 0$. In order to compare with their data we had to match the parameters of our pulse sufficiently well with theirs. For their calculation they assumed an intensity of $I = 10^{16} \frac{W}{cm^2}$ and a pulse duration of 3 fs. For our calculation we assumed an intensity of $I = 5 \times 10^{15} \frac{W}{cm^2}$ and a pulse duration of 20 cycles, which ends up being about 3.73 fs. The results of our calculation and that of Saalman et al. are compared below.

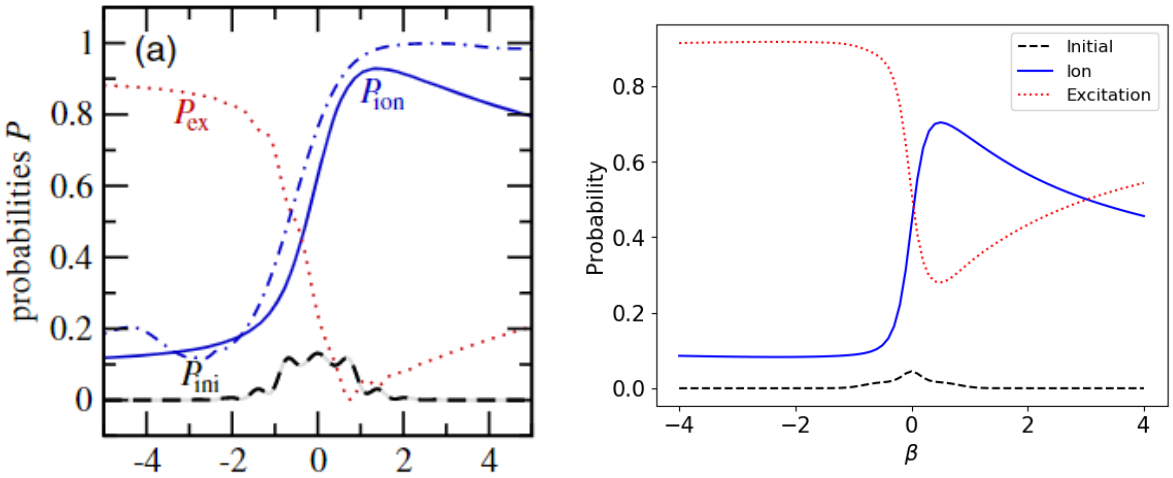

Figure 1.4: Comparison of the results for ionization (solid line), excitation to $2p$-state (dotted line) and initial state population (dashed line) by Saalmann et al. (left) with those of our simulations (right). The pulse parameters in both calculations were similar (see text).

From this comparison we are able to see that all of the features of their results are clearly present in ours as well. We see ionization is enhanced/suppressed in the same regions, the ground

state population is symmetric in β, and the excitation probability to the $2p$ state that is almost a mirror image of the ionization probability. We have therefore successfully replicated the results for the long pulse limit, and we now seek to analyze the new data that presents itself for calculations with shorter pulse durations.

Chapter 2

Results and Discussion

2.1 Population Control via Chirp for Ultrashort Pulses

Since the goal of this study is to see how the resultant Helium state populations change with respect to both chirp parameter β as well as the number of pulse cycles N, we have simulated the interaction with the laser pulses over a suitable range of parameters. We took sample pulse durations at $N = 2, 4, 6, 8, 10, 12, 15$, and 20. This range will allow us to see how the populations for long pulses at $N = 20$ varies towards the populations seen for the $N = 2$ result. For the chirp parameter we restricted the range to $\beta \in [-4, 4]$ which is the same range over which the chirp was varied for the long pulses in [1]. To start analyzing our results we show in Fig. 1.4 the results of the numerical simulations for the $N = 2$ case.

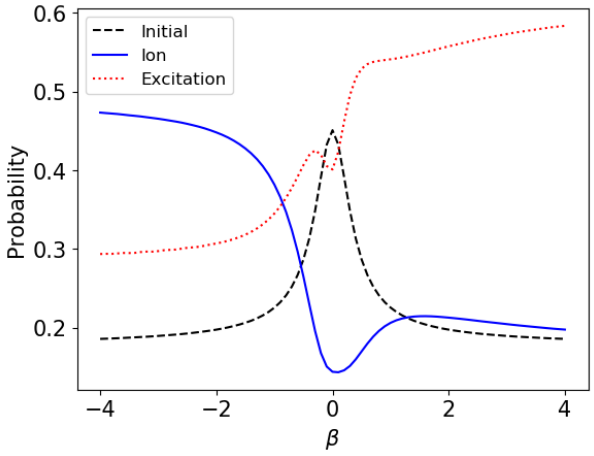

Figure 2.1: Ionization, excitation and ground state populations in Helium after interaction with a pulse for $N = 2$, as a function of the chirp parameter β.

The first thing to note from this plot is that the suppression and promotion of ionization is very different for the interaction with the ultrashort pulse as compared to the 20 cycle results (Figure 1.4). Instead of ionization being suppressed for $\beta < 0$ it is now promoted, while we find the ionization suppression region for $\beta > 0$. We also note that while ionization is promoted in the negative chirp parameter region, instead of ionization reaching around 90 percent, it is now enhanced to just below 50 percent. Thus, we see that the ability to control ionization changes significantly when the pulse duration is reduced to few cycles.

Now, focusing on Figure 2.1, we further see a more complex structure in how the populations vary with chirp parameter as compared to the long pulse result from [1] in Figure 1.4. The ionization population now has a local minimum at $\beta = 0$, which was not present in previous calculations. This minimum value is approximately zero, even lower than in the suppressed region. Although this is interesting, since we are focused on the interaction with chirped pulses we will not discuss characteristics at $\beta = 0$ in much detail. We also see that the ground state population is still symmetric with respect to the chirp parameter, however the peak value at $\beta = 0$ has increased to almost 45 percent. The final observation which we would like to point out is in regards to the excitation probability, which we see is no longer a mirror image of the ionization probability. This seems to be correlated with the large peak in ground state population mentioned previously, however this correlation does not readily explain the variety of maxima and minima observed in the plot, specifically at around $\beta = -0.5$.

In order to find trends in the changes in the results when the pulse duration is reduced from long to ultrashort pulses and seek for insights behind the physical phenomena behind the change in populations, we now turn our attention to the results for $N = 8$ and $N = 15$. We see in the results shown in Fig. 2.2 that for the longer pulse duration $N = 15$ (panel on the left), we still have ionization suppression for $\beta < 0$, however the population in the promoted region is less significant than for the $N = 20$ result. We also see that the ground state population at $\beta = 0$ has not increased yet. For the $N = 8$ case (panel on the right), it acts much more as an intermediate between $N = 2$ and $N = 20$. The ionization population still retains a similar dependence to the $N = 20$ case;

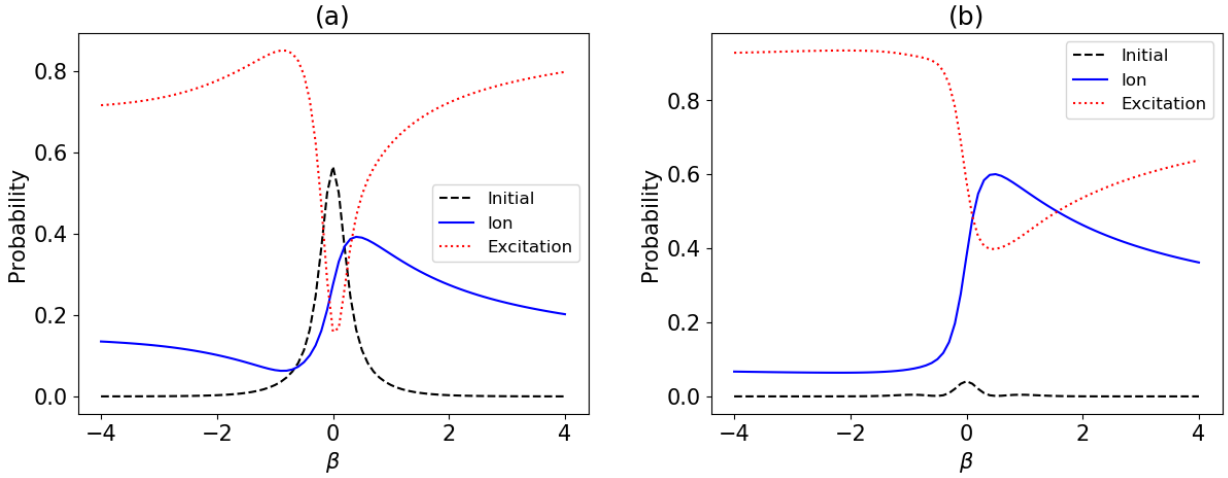

Figure 2.2: Same as Figure 2.1 but for $N = 15$ (a) and $N = 8$ (b).

however the maximum population reached is much smaller. We also see that the ground state population spike has increased to around 60 percent, even larger than in the $N = 2$ result. Overall there is a much new structure that occurs throughout these plots which was not observed previously for the long pulses. In the rest of this thesis we now focus on identifying a mechanism which has the potential to explain specifically the change for the ionization enhancement and suppression in the different chirp region that we have noted in these plots.

2.1.1 Time Order of Population Transfer to Different States

The mechanism we propose is related to how the central frequency changes over the duration of the pulse depending on the sign of β and how this impacts the population of bound and continuum states. Thus we start by looking at how the instantaneous frequency changes with time. As discussed in the background section, the instantaneous frequency is not entirely determined by the argument of the carrier wave of the pulse. It is also determined by the localization in time caused by the envelope function, which introduces a width to the frequency spectrum. To visualize this aspect we plot the central frequency vs. time in Figure 2.3 for $\beta = -4$ (a) and $\beta = -4$ (b) and a 2 cycle pulse.

In these plots we present the central frequency, defined as the derivative with respect to time of the angle ϕ inside the argument of the carrier wave. In order to represent the Fourier broadening of the frequency spectrum in the pulse, which has been discussed in the background section, we have plotted the frequency spectrum as a thick line which fades out towards the edges. The width of the faded area above/below the central frequency represents one half of the FWHM. This implies that the entire width of the frequency line is the FWHM. This allows us to visualize how strongly the frequency overlaps with some of the coupling frequencies. In these plots we also have some supplemental information shown, such as the relative intensity represented by the envelope function. We have also plotted the coupling frequency between the ground state and various excited states and the ionization frequency via the dotted lines.

Focusing first on the $\beta = 4$ plot (right panel), we see that the frequency starts very far

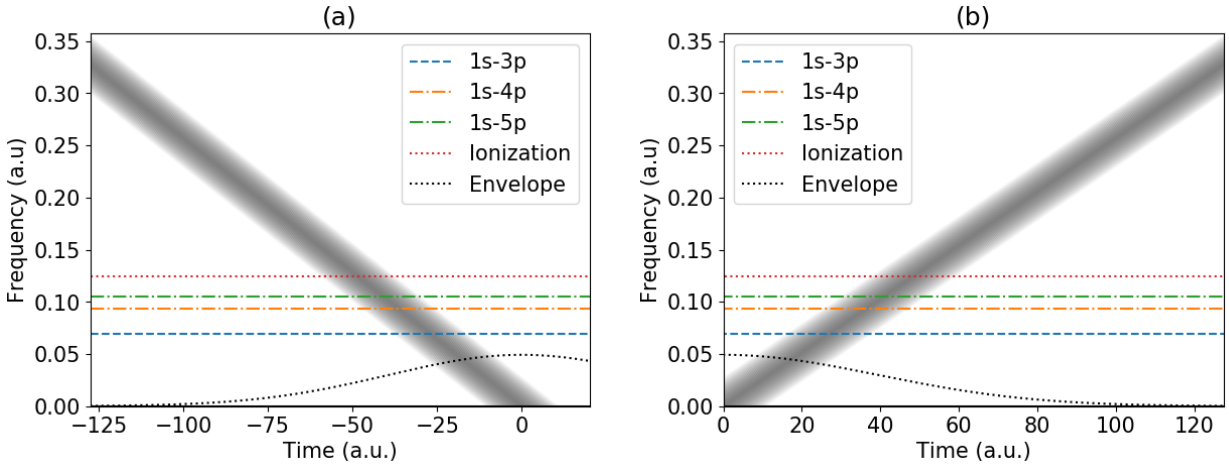

Figure 2.3: Change of frequency spectrum of an ultrashort 2 cycle pulse as a function of time for (a) $\beta = -4$ and (b) $\beta = +4$. The shaded area resembles the width of the frequency spectrum and the horizontal lines correspond to the transition energies to different p-states as well as the ionization energy in Helium. Also shown, is the envelope of the ultrashort laser pulse.

below the unchirped frequency, which corresponds to the $1s - 2p$ state coupling. This means that population transfer from the ground state to any excited state or the continuum is not promoted until half way through the pulse. Close to the peak of the pulse the frequency spectrum begins to overlap with the coupling frequencies in order of increasing energy, finally surpassing the ionization threshold. For this scenario we therefore expect that there is a very small amount of population should be leaving the ground state until $t = 0$, at which point the field can induce the $1s - 2p$ resonant transition with almost all of the population still in the $1s$ state.

Turning our attention to the $\beta = -4$ plot in Figure 2.3 (a), we see that at the start of the pulse the frequency is much larger than even the ionization threshold. Thus, as soon as the pulse begins interacting with the Helium atom population is being transferred from the ground state. At first there is predominantly ionization, then as time progresses the frequency drops below the ionization threshold. From this point on bound states are being more and more populated. However, by this time the ground state population has already faced depletion to the continuum. We therefore see that the mechanism in how states are populated is very different and linked to the idea that there are no coupling frequencies below the $1s - 2p$ coupling, since there are no more accessible energy eigenstates below the $2p$ state. We therefore expect that the time ordering of population transfer may provide an explanation for the results in an ultrashort pulse. Based on the dependence of the frequency on the time, we expect the ionization probability to be very large for $\beta = -4$ and very small for $\beta = 4$. Comparing to Figure 2.1, not only do we see this is true, but it is the exact ionization behavior that we have been referring to as suppression and enhancement. We now demonstrate the predictive power of this idea through a specific example for the $3p$ state population.

2.2 $3p$ State Population

In order to show how this model can be used to explain the new results, we will reduce the scope of our analysis by looking at the behavior of a single population at a specific chirp parameter. Once these are fixed, we then vary the duration of the pulse to see if there is an identifiable pattern than we can try and predict using the model. A good choice to test our model is the $3p$ population

at $\beta = -4$. This is because the behavior of the population in the vicinity of $\beta = -4$ is not very complex, and because the population has a rather smooth pattern when plotted against pulse duration. Since the model we are proposing relies on the population of other states before (or after) the $3p$ resonance is reached, it is also important to plot the higher and lower energy state population versus time as well. All of this information is shown in Figure 2.4.

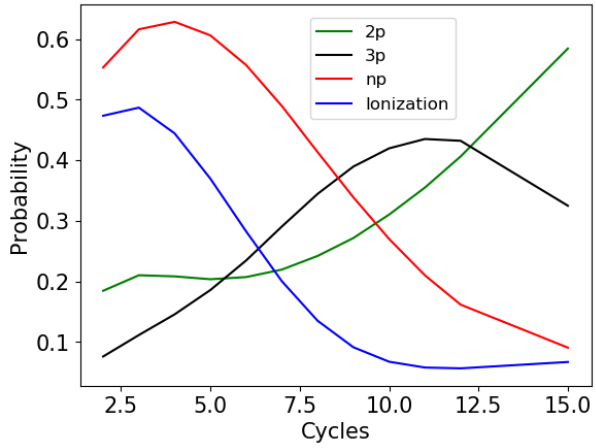

Figure 2.4: Ionization, higher excited state, $3p$ state, and $2p$ state population as a function of pulse duration for a chirp parameter of $\beta = -4$.

In Figure 2.4 we see that the $3p$ population at $\beta = -4$ attains its maximum value at around $N = 12$. As the pulse duration increases or decreases away from $N = 12$ the $3p$ population decreases. Furthermore shown in this plot are the $2p$ population, np population, and the ionization probability. The np population in this plot is the total population in all excited bound states above the $3p$ state, so the the sum of the $4p, 5p, 6p$ etc. population. From this plot we see that both the ionization and higher excited state populations have their maximum value for the shortest pulse duration, and then decrease significantly as N increases. This is in contrast to the $2p$ state population, which does not increase much for increasing pulse duration until about $N = 8$. If the model is correct, then we would expect that the frequency versus time dependence should let us explain why the populations have these specific patterns. This would be a good indicator that the model can be used to explain characteristics of other state populations as well. To start the analysis we refer to the frequency versus time plot for the shortest pulse $N = 2$ in Figure 2.3 (right panel) and see if

the information it provides can explain what we observe in Figure 2.4.

We start by explaining why the $3p$ state population for $N = 2$ is much lower than the $N = 12$ result. From Figure 2.3 (right) we see that at the beginning of the pulse the central frequency is above the ionization threshold, and stays above the threshold for almost the whole rising part of the pulse. This is consistent with Figure 2.4, where the ionization probability is almost 50 percent for $N = 2$. Since the continuum is populated first, a large amount of the population is transferred from the ground state before it has the chance to be transferred to the $3p$ state. We can understand this phenomenon more clearly by plotting the number of cycles for which the various populations achieve their maximum values in Figure 2.5.

Figure 2.5: Number of cycles N at which maximum population for various states in Helium is reached in a chirped pulse with $\beta = -4$.

There is a very distinct trend in these results. As we consider higher energy bound states, the pulse duration at which maximum population is reached decreases. In order to explain why this happens with the proposed model, we need to plot the frequency versus time curve at $\beta = -4$ for various pulse durations. In doing so, we should also be able to explain why the $3p$ population reaches its local maximum at around $N = 12$. To start the analysis we plot the frequency versus time curve for three different pulse durations below in Figure 2.6.

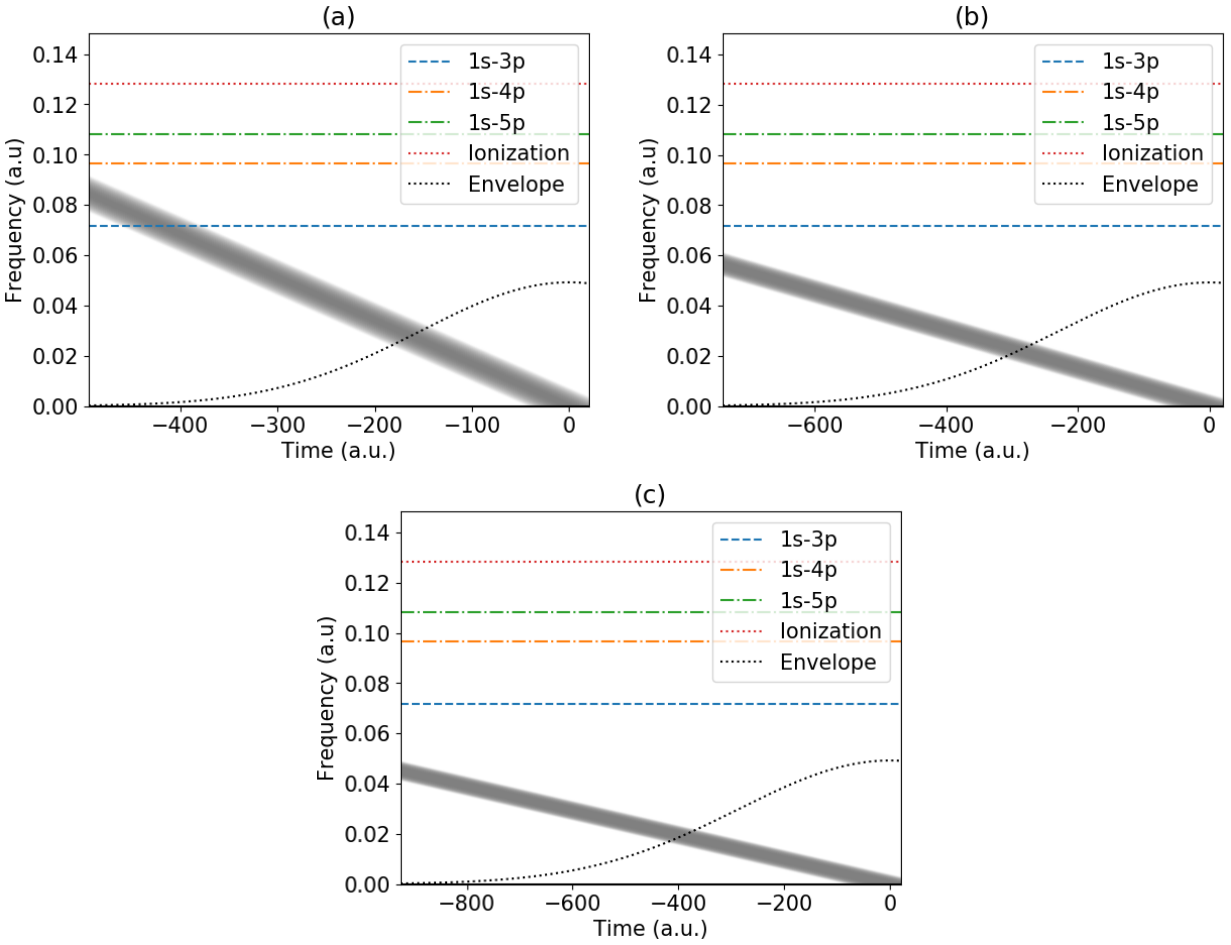

Figure 2.6: Same as Figure 2.3(a) but for (a) $N = 8$, (b) $N = 12$, and (c) $N = 15$ for $\beta = -4$.

First we explain why the higher energy states achieve their maximum population value for smaller values of N. To this end, we note from Figure 2.6 that as the pulses become longe,r the central frequency at the beginning of the pulse decreases and the spectral width decreases. As a consequence, higher frequency/energy components are no longer contributing as much. and higher energy couplings are no longer possible in long pulses. As the higher energy couplings become impossible, less population is transferred to these states allowing more population to be transferred to lower energy states and lower energy states achieve their maximum for longer pulses. The net result is that as pulse duration increases we are preventing higher energy state couplings from being reached.

We now more specifically use the information shown in Figure 2.7 to explain the the $3p$ result. First, we note that for $N = 8$ the initial central frequency of the pulse is no longer above the ionization threshold. Instead, the central frequency now starts just above the $1s - 3p$ resonance at the beginning of the pulse. Based on this observation, we can argue that there is very small amount of population being ionized (or transferred to higher energy states) before the $3p$ state is being populated. This in turn allows for more population to me moved to the $3p$ state, explaining why the $3p$ population further increases as we approach $N = 12$. Now looking at the $N = 15$ plot, the initial frequency of the pulse has dropped even further, below the $1s - 3p$ coupling. This implies that the resonance condition to get efficient population transfer between the ground state and the $3p$ state is barely reached, even though there should be more than enough population in the ground state to transfer. Consequently, the final $3p$ population for a $n = 15$ pulse is smaller than for $N = 12$.

We can also analyze the frequency vs. time plot for $N = 12$ to further explain why the maximum occurs at (or just before) that specific value of N. From this plot we see that the initial frequency starts just below the $1s - 3p$ resonance. This means that in the vicinity of $N = 12$, the initial central frequency of the pulse is exactly equal to the $1s - 3p$ transition energy. This would mean that at as soon as the pulse begins interacting with the Helium atom, efficient population transfer between the $1s$ and $3p$ state would occur, while higher energy states are never in resonance with the central frequency. The fact that the initial frequency is just below the coupling might

indicate that the true maximum is for an N slightly smaller than 12, which would have been missed due to the sampling choice for N values. This is consistent with Figure 2.4, where we can see that the true maximum occurs just before $N = 12$.

We have therefore been able to explain the characteristics of the $3p$ state population by considering only the frequency vs. time curve, and how it relates to various coupling frequencies. We now turn to discussing some other cases where this argument works well to display its breadth and predictive ability for both other state populations as well as different chirp parameters.

2.3 Additional Evidence

We have shown that the proposed model works in explaining the $3p$ state population at $\beta = -4$. Since it has shown promise for this specific case, we can try to broaden our considerations. To this end, we investigate the $3p$ population for another chirp parameter, namely $\beta = -1$ and the behavior of the $2p$ population at $\beta = -4$. By looking at these two cases we display that this model has potential to explain not only other population trends, but also that it can be applied to chirp parameters other than $\beta = -4$.

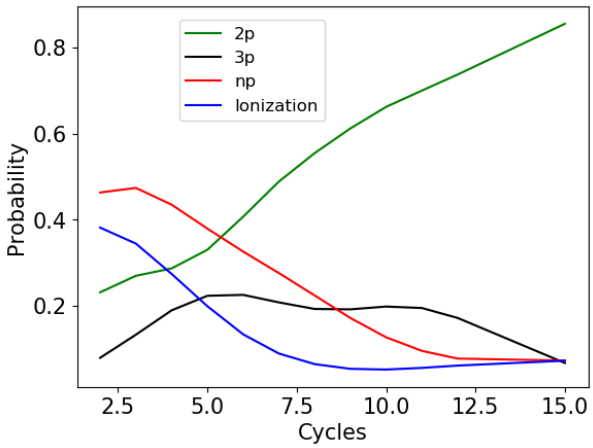

Figure 2.7: Same as Figure 2.6 for β = -1.

To start this discussion we consider the $3p$ population for $\beta = -1$ and see how the population varies with the pulse duration. This information is shown in Figure 2.7. We can see how the

population trends are different compared to the $\beta = -4$ result. The ionization for the shortest pulses is smaller, starting at around 25 percent as opposed to the roughly 50 percent value we observed in the $\beta = -4$ case. We also see that the $3p$ population only reaches a maximum of about 20 percent, and that instead of reaching the maximum value around $N = 12$, the maximum appears at about $N = 6$. We now turn to analyzing the frequency vs. time plot to explain these observations.

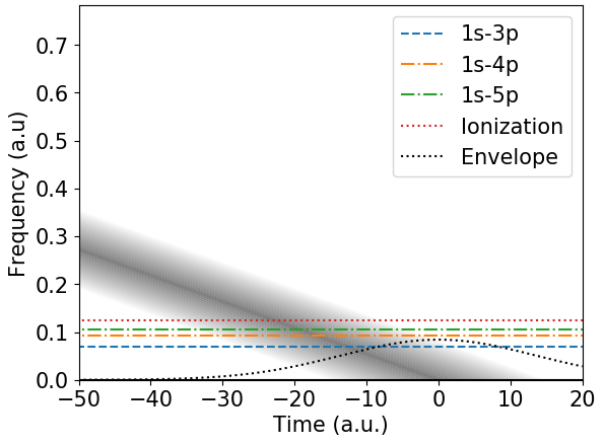

Figure 2.8: Frequency versus time plot for $N = 2$ and $\beta = -1$

First, we explain the low ionization observed for the $N = 2$ results. From Figure 2.8 we see that the frequency begins at about 0.3 a.u., which is approximately the same starting frequency that we observed for the $\beta = -4$ case. However, the difference lies in the duration over which the frequency is above the ionization threshold. To compare, we see that the frequency is only above the ionization threshold for approximately 25 a.u., as opposed to the over 75 a.u shown in Figure 2.3. This difference in time scale over which ionization is most likely can therefore explain why the ionization population has dropped significantly.

Next, we explain why the maximum value for the population transfer into the $3p$ state is reached at $N = 6$. To this end, we present in Figure 2.8 the time vs. frequency plot and see that the $1s - 3p$ coupling frequency is reached at the start of the pulse. This is exactly the same situation that we have identified for the maximum value in the $3p$ population for $\beta = -4$ at $N = 12$. To reconcile, the pulse begins with the frequency resonant with a population transfer from the $1s$ into

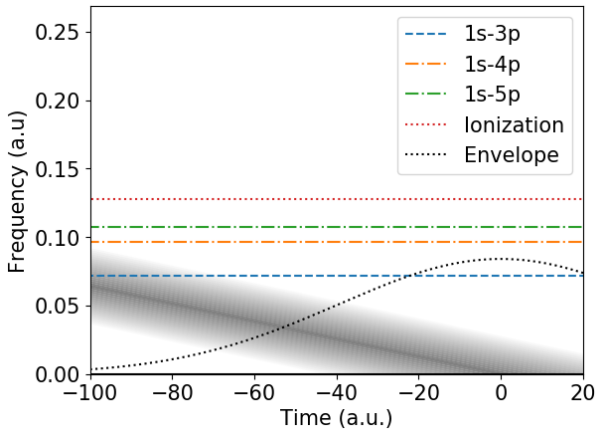

Figure 2.9: Same as Figure 2.6. but for $N = 6$ and $\beta = -1$.

the $3p$ state, before any population has been transferred from the ground state, allowing maximum population to be moved to the $3p$ state.

Finally, we turn our attention to the $2p$ state population for the case of $\beta = -4$. This discussion is distinct from our discussion on the $3p$ state, since the pulse is guaranteed to overlap with the $1s - 2p$ coupling by design at $t = 0$. In fact, in our previous discussions we found that as the pulses become longer in time, the initial frequency of the pulse decreased. Since for the longest pulses only the $1s - 2p$ coupling should be met, we would expect increasingly efficient population transfer from the ground state to the $2p$ state as longer is the pulse. To see if this is correct we focus on the $2p$ population in Figure 2.4. From this figure we see that it is indeed true that the $2p$ state population is increasing as pulse duration increases. In fact, we expect that for the longest pulses, we may start approaching the long pulse limit where extremely efficient population transfer between the ground state and the $2p$ state is achieved.

2.4 Conclusions

The goal of this study was to simulate the interaction of Helium with ultrashort intense linearly chirped laser pulses. By simulating over a wide range of pulse durations we were able to see how the population for the shortest and longest pulses differ, and attempt to explain why the final populations have the patterns that we observed. Using the frequency versus time plots for various chirp parameters and pulse durations we have been able to explain several patterns and trends in the final population distributions of the Helium atom. We have showcased the predictive aspect of the model by explaining why higher energy states achieve their maximum population for shorter pulses, why the $3p$ population at $\beta = -4$ and $\beta = -1$ achieves its maximum value around $N = 12$ and $N = 5$ respectively. Finally, we have shown that the longer pulse results are consistent with efficient population transfer to the $2p$ state that we expect in the long pulse limit. All of these examples display that by only considering the frequency and state couplings many characteristics can not only be explained, but predicted. The result of this study may help to understand how quantum systems can be manipulated via interaction with light, which is important to open doors

for future predictions and applications of this model.

Bibliography

[1] S. Cong, Control of quantum systems: theory and methods. Singapore: John Wiley & Sons Inc, 2014.

[2] N. V. Vitanov, T. Halfmann, B. W. Shore, and K. Bergmann, "Laser-induced population transfer by adiabatic passage techniques," Annual Review of Physical Chemistry, vol. 52, pp. 763–809, 2001.

[3] M. Shapiro, P. Brumer, and M. Shapiro, Quantum control of molecular processes. Weinheim: Wiley-VCH, 2nd, rev. and enl. ed ed., 2012. OCLC: ocn751755101.

[4] S. A. Rice and M. Zhao, Optical control of molecular dynamics. The George Fisher Baker non-resident lectureship in chemistry at Cornell University, New York: John Wiley, 2000.

[5] N. V. Vitanov, A. A. Rangelov, B. W. Shore, and K. Bergmann, "Stimulated Raman adiabatic passage in physics, chemistry, and beyond," Reviews of Modern Physics, vol. 89, p. 015006, Mar. 2017.

[6] U. Saalmann, S. K. Giri, and J. M. Rost, "Adiabatic Passage to the Continuum: Controlling Ionization with Chirped Laser Pulses," Physical Review Letters, vol. 121, p. 153203, Oct. 2018.

[7] S. I. Hwang, S. B. Park, J. Mun, W. Cho, C. H. Nam, and K. T. Kim, "Generation of a single-cycle pulse using a two-stage compressor and its temporal characterization using a tunnelling ionization method," Scientific Reports, vol. 9, p. 1613, Dec. 2019.

[8] R. N. Coffee, J. P. Cryan, J. Duris, W. Helml, S. Li, and A. Marinelli, "Development of ultrafast capabilities for X-ray free-electron lasers at the linac coherent light source," Philosophical Transactions of the Royal Society A: Mathematical, Physical and Engineering Sciences, vol. 377, p. 20180386, May 2019.

[9] R. Reiff, T. Joyce, A. Jaroń-Becker, and A. Becker, "Single-active electron calculations of high-order harmonic generation from valence shells in atoms for quantitative comparison with TDDFT calculations," Journal of Physics Communications, vol. 4, p. 065011, June 2020.

[10] J. Venzke, A. Jaroń-Becker, and A. Becker, "Ionization of helium by an ultrashort extreme-ultraviolet laser pulse," Journal of Physics B: Atomic, Molecular and Optical Physics, vol. 53, p. 085602, Apr. 2020.

[11] Y.-C. Han and L. B. Madsen, "Comparison between length and velocity gauges in quantum simulations of high-order harmonic generation," Physical Review A, vol. 81, p. 063430, June 2010.

[12] L. D. Dalcin, R. R. Paz, P. A. Kler, and A. Cosimo, "Parallel distributed computing using Python," Advances in Water Resources, vol. 34, pp. 1124–1139, Sept. 2011.

[13] S. Behnel, R. Bradshaw, C. Citro, L. Dalcin, D. S. Seljebotn, and K. Smith, "Cython: The Best of Both Worlds," Computing in Science & Engineering, vol. 13, pp. 31–39, Mar. 2011.